Eigenstrain Techniques for Modeling Adaptive Structures: II. Active Damping

Abdulmalik A. A. Alghamdi and Abhijit Dasgupta

Journal of Intelligent Material Systems and Structures 2000; 11; 631
DOI: 10.1106/NYLF-WKYV-UUWX-RPV9

Eigenstrain Techniques for Modeling Adaptive Structures: II. Active Damping

ABDULMALIK A. A. ALGHAMDI[1,*] AND ABHIJIT DASGUPTA[2]

[1]*Department of Production Engineering and Mechanical Systems Design, King Abdulaziz University, Jeddah 21413, Saudi Arabia*

[2]*Department of Mechanical Engineering, University of Maryland, College Park, MD 20742*

ABSTRACT: This is the second paper, in a two-part series, that demonstrates the utility of Eshelby's eigenstrain techniques for modeling adaptive structures. The first paper addressed adaptive stiffening (Alghamdi and Dasgupta, 2000). The objective of this second paper is to model adaptive damping. Distributions of small active piezoceramic devices embedded in the adaptive structure are treated as elastic heterogeneous inclusions. Sensors are treated as elastic heterogeneities subjected to external loads, whereas actuators are modeled as elastic heterogeneities subjected to both external loads and internal induced strains caused by the converse piezoelectric effect. The coupled electromechanical boundary value problem is solved using a generalized form of Hamilton's principle where the energy functional is evaluated using the eigenstrain method. System dynamic equations are developed for active damping and a numerical solution to the variational problem is obtained by using the Raleigh-Ritz approach. Numerical results are verified experimentally using a cantilever beam with distributions of embedded piezoelectric (PZT-5H) mini-devices. A significant amount of damping is achieved for low volume fraction of devices and good agreement is obtained between numerical and experimental results. The eigenstrain technique is demonstrated to be a capable three-dimensional tool for modeling adaptive structures with embedded distributions of mini-devices.

INTRODUCTION

An adaptive structure can be defined as a system that has the capability of sensing a stimulus and responding to it in an appropriate fashion. So, the concept pre-supposes that the structure has sensors, actuators and logic controllers. Developments in the area of adaptive material systems and structures have resulted in significant theoretical and experimental investigations of adaptivity phenomena. Adaptive structures have been used in different areas such as vibration control (Baz and Ro, 1995), rotorcraft (Chen and Chopra, 1996), aircraft structures (Crawley, 1994), structural dynamics (Chandrashekhara and Bhatia, 1993), robotics (Yoshida, Nenchev and Uchiyama, 1999), civilian structures (Soh et al., 2000), biomechanics (Kupchinov et al., 1993), etc.

Several active materials have been used in adaptive structures including, piezoelectrics, shape memory alloys, electrostrictives and magnetostrictives. However, piezoelectric materials have attracted significant attention for their potential application as sensors and actuators for controlling the response of active structures, mainly because of their moderate actuation authority, high frequency response and ease of control.

Most of the current adaptive structure applications utilize fairly large devices, compared to the characteristic length scale of the host structure, in order to achieve adequate authority. The obtrusivity of such large devices is known to cause local perturbation of stress and strain fields in the host, thus creating the possibility of initiating local damage and compromising the structural integrity of the devices. One possible way to minimize the obtrusivity is to reduce the size of the devices, to distribute them throughout the volume of the host, and to increase their number as required, to achieve the desired authority. Distributing the devices throughout the volume also provides certain advantages from the perspective of distributed control strategies. However, embedding of small devices produces three-dimensional stress interactions that are more difficult to model than those arising in surface-mounted devices and there is a lack of generic modeling techniques for such structures in the open literature.

There have been numerous studies in the literature for modeling mechanical interactions between devices (sensor/actuator) and host in adaptive structures. The interaction mechanics of active elements in adaptive structures have been analyzed by using simple beam models (Bailey and Hubbard, 1985), pin force models (Crawley and de Luis, 1987), large deformation beam theory (Im and Atluri, 1989), laminate analysis (Crawley and Lazarus, 1991), nonlinear analysis (Pratt, Queine and Nayfah, 1999), and one-dimensional eigen-function approximations (Lin and Rogers, 1992). Other numerical approximation methods have also been developed to model the coupled boundary value problems in active structures. These include finite element meth-

*Author to whom correspondence should be addressed. E-mail: aljinaidi@hotmail.com

1530-8138/00/08 0631-11 $10.00/0 DOI: 10.1106/NYLF-WKYV-UUWX-RPV9

ods (Allik and Hughes, 1970; Mahut, Agbosou and Pastor, 1998), Rayleigh Ritz methods (Hagood, Chung and Flotow, 1990) and strain energy methods (Wang and Rogers, 1991; Chee, Tong and Steven, 1998). In this paper, the mechanical interaction between the devices and the host is modeled using eigenstrain analyses that have been introduced in a previous paper (Alghamdi and Dasgupta, 2000). The volume fraction (V_f) of these devices is less than 2% of the structure volume.

The equivalent-inclusion technique (Eshelby, 1957) is a powerful and unified solution method capable of solving the elastic problem of an anisotropic heterogeneity inside an isotropic, infinite matrix. This method is brought to adaptive structures to model the elastic interaction between actuators/sensors and the host, by using appropriate Green's functions. The energy formulation of the eigenstrain method is made possible by adapting a generalized Hamilton's principle, and numerical solutions are obtained using the Rayleigh-Ritz technique.

A one-dimensional beam problem is investigated both analytically and experimentally and the adaptivity of the beam is illustrated through active damping of a cantilever beam, using velocity feedback control. Experimental verification of the analytical model is presented for a cantilevered Alplex beam containing distributions of small, embedded PZT-5H sensor/actuator mini-devices.

ANALYSIS

An adaptive structure with multiple embedded mini-devices is modeled as a large elastic matrix with embedded ellipsoidal elastic heterogeneities, as shown in Figure 1. Host and device materials are approximated to be isothermal, linear and mechanically isotropic. Although the eigenstrain techniques can handle any coupled-energy problem, only an electro-mechanical energy problem with piezoelectric material for the devices is being formulated here.

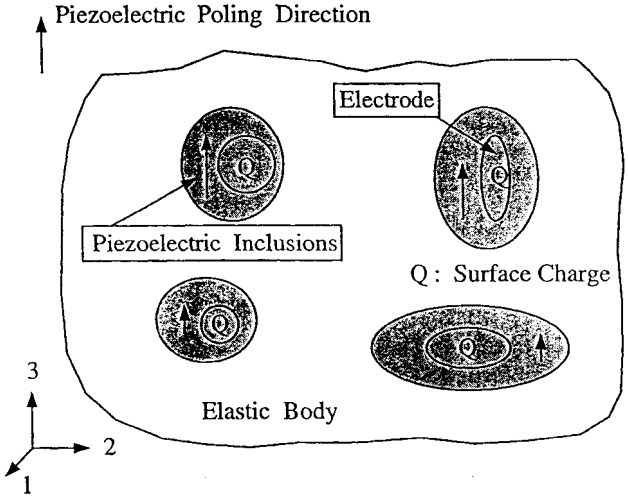

Figure 1. *Active structures.*

The mechanical, electro-mechanical and electrical energy of the adaptive structure are computed using a generalized form of Hamilton's principle (Tiersten, 1969),

$$\delta\int_{t_0}^{t} L\,dt + \delta\int_{t_0}^{t} W\,dt = 0 \tag{1}$$

where L is the Lagrangian functional, which is the difference between the kinetic energy and the electric enthalpy; δ is the variational operator; W is the external work term; and (t_0, t) defines the time interval over which stationary values are sought.

The linearized, isothermal, coupled, electro-mechanical constitutive model for piezoelectric structures is given by (Ikeda, 1990)

$$\sigma_{ij} = C_{ijkl}\varepsilon_{kl} - e_{kij}E_k \tag{2}$$

$$D_i = e_{ikl}\varepsilon_{kl} + \varepsilon^s_{ij}E_j \tag{3}$$

where σ_{ij} is the stress tensor, D_i is the electrical displacement vector, ε_{kl} is the strain tensor, E_k is the electrical field vector, C_{ijkl} is the mechanical stiffness tensor evaluated at constant (zero) electrical field, e_{ijk} is the piezoelectric stress coupling tensor, and ε^s_{ij} is the dielectric permittivity tensor evaluated at constant (zero) strain.

Taking the first variation inside the volume and surface integrals with respect to the primary variables (displacement u_i and potential V) one can get,

$$\int_{t_0}^{t}\left[\int_v \ddot{u}_i\rho\delta u_i dv + \int_v \varepsilon_{ij}C_{ijkl}\delta\varepsilon_{kl}dv - \int_\Omega \varepsilon_{ij}e_{kij}\delta E_k dv - \int_\Omega \delta\varepsilon_{ij}e_{kij}E_k dv - \int_\Omega E_i\varepsilon_{ij}\delta E_j dv - \int_s Q\delta V dA\right]dt = 0 \tag{4}$$

where ρ is the density, v is the volume of the beam, Ω is the volume of the devices, Q is the specified surface charge density and S is the electrode surface area of the devices. This is the electro-mechanical variational equation governing the adaptive structure consisting of the host and embedded piezoelectric devices. The integration domain in the above equation covers the host, sensors, and actuators.

The eigenstrain technique is applied to obtain the elastic interaction fields, both in the host and the devices, under internal actuation load (in the actuator, due to piezoelectricity effect) and external applied loads (Dasgupta and Alghamdi, 1993). The eigenstrain method for modeling the disturbance field is based upon modeling the heterogeneity problem as an equivalent inclusion in a homogeneous media with a fictitious eigenstrain ε^f_{ij} prescribed in the inclusion, so as to produce the same stress field in Ω as the original heterogeneity, under both external loads and internal actuation strains. The

stress inside the heterogeneity is written, using Hooke's law as,

$$\sigma_{ij} = \sigma^0_{ij} + \sigma'_{ij} = C^d_{ijkl}(\varepsilon^0_{kl} + \varepsilon'_{kl} - \varepsilon^a_{kl})$$
$$= C_{ijkl}(\varepsilon^0_{kl} + \varepsilon'_{kl} - \varepsilon^*_{kl}) \quad (5)$$

where $\varepsilon^*_{ij} = \varepsilon^f_{ij} + \varepsilon^p_{ij}$ and superscript d on the stiffness indicates the device, and superscripts 0, /, a, *, f and p on the stress and strain terms indicate applied far-field value; disturbance due to the presence of the heterogeneity and the induced strain; induced strain inside the actuator; total eigenstrain; fictitious eigenstrains due to external load; and the applied eigenstrains due to the induced strain; respectively. Details of these terms can be found in Alghamdi (1995).

The mechanical strain inside the devices can be calculated as,

$$\varepsilon_{ij} = \varepsilon^0_{ij} + S_{ijkl}\varepsilon^*_{kl} \quad (6)$$

where S_{ijkl} is Eshelby's fourth-order strain concentration tensor (Alghamdi and Dasgupta, 2000). Note that the total strain in Equation (6) is the strain inside the actuator, and consists of two parts, the far-field strain and the eigenstrain. In this analysis, both sensors and actuators have a fictitious eigenstrain due to the external far-field loads, while the actuators have additional real eigenstrains due to the converse effect of the actuation voltage.

For the media (host) only the far-field strain is considered, while for sensors far-field strain is considered in addition to the fictitious eigenstrain (i.e., there is no applied eigenstrain: $\varepsilon^p_{ij} = 0$). The real eigenstrains due to the direct piezoelectric effect at the sensor and actuator are ignored because of their negligible magnitude in comparison to that associated with the converse piezoelectric effect due to the excitation voltage.

The elastic energy term in Equation (4) can be written in terms of the eigenstrain as (Alghamdi and Dasgupta, 1993a),

$$\int_v \varepsilon_{ij}C_{ijkl}\delta\varepsilon_{kl}dv = \int_v \varepsilon^0_{ij}C_{ijkl}\delta\varepsilon^0_{kl}dv + \int_\Omega \varepsilon^*_{ij}C_{ijkl}S_{klmn}\delta\varepsilon^*_{mn}dv$$
$$+ \int_\Omega \varepsilon^0_{ij}\Delta C_{ijkl}\delta\varepsilon^0_{kl}dv + \int_\Omega \varepsilon^0_{ij}\Delta C_{ijkl}S_{klmn}\delta\varepsilon^*_{mn}dv$$
$$+ \int_\Omega \delta\varepsilon^0_{ij}\Delta C_{ijkl}S_{klmn}\varepsilon^*_{mn}dv + \int_\Omega S_{ijmn}\varepsilon^*_{mn}\Delta C_{ijkl}S_{klpr}\delta\varepsilon^*_{pr}dv \quad (7)$$

where $\Delta C_{ijkl} = C^d_{ijkl} - C_{ijkl}$. Equation (7) gives the strain energy of adaptive structure with multiple embedded devices subjected to uniform far-field and uniform applied strain in actuators. Note that the total strain energy can be obtained without solving the perturbation introduced in the host by the mechanical field in the heterogeneity. Uniform and linear far-field and applied eigenstrain loadings have been investigated by Alghamdi and Dasgupta (1993b).

RAYLEIGH-RITZ APPROXIMATION

In this section the dynamic behavior of a sample adaptive structure is presented by implementing the variational scheme given above with the eigenstrain analysis. The adaptive structure selected for this study is a cantilever beam made of Alplex plastic with embedded piezoceramic devices (see Figure 2). The beam contains two rows of uniformly spaced mini-devices arranged symmetrically with respect to the neutral plane. One row contains all sensors and the other contains all actuators. The analysis presented in this paper is not limited to this type of structure, but it can be used to model any structure by assuming appropriate displacement functions. For illustrative purposes, only the first vibrational mode is considered.

As the beam flexes, the sensor outputs are used in a closed-loop constant-feedback-gain control circuit to activate the corresponding actuator on the opposite side of the neutral axis. If the voltage supplied is made proportional to the sensor output voltage, then the result is an apparent stiffening of the structure with an accompanying increase in the natural frequency (Alghamdi and Dasgupta, 2000). If the input voltage is made proportional to the time-derivative of the sensor output voltage (actuation strain is made proportional to the bending strain rate), then the result is an apparent adaptive damping of the structure.

For simplicity, we assume a Euler-Bernoulli cantilever beam, no rotary inertia, perfect bond condition, and no electrical losses. In accordance with Rayleigh-Ritz techniques, the transverse displacement function (w) for the first vibrational mode for the cantilever beam is assumed to be sinusoidal in the y-z plane:

$$w(y,t) = \left[1 - \cos\left(\frac{\pi y}{2l}\right)\right] r(t) \quad (8)$$

where t is time, the y-axis is oriented along the length of the beam (see Figure 2), l is the beam length, and $r(t)$ is a generalized mechanical degree-of-freedom representing the tip displacement. For simplicity, sinusoidal function is selected to provide an approximate shape of the beam deflection. However, generic beam functions can be used to get better approximation of the beam deflection (Gartner and Olgac, 1982). The displacement field in Equation (8) is used as the

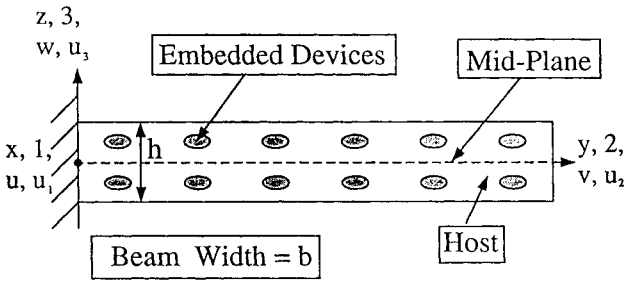

Figure 2. *Schematic drawing of the adaptive cantilever beam.*

far-field boundary condition, ε_{ij}^{0}, for the eigenstrain analysis in Equation (7).

By assuming uniform electrical field in the sensor, the derivative of the sensor voltage can be written in terms of the assumed displacement function (Alghamdi, 1995)

$$\dot{V}_s(x,t) = z_m \frac{\pi^2}{4l^2} \cos\left(\frac{\pi y_m}{2l}\right) h_{3ij}\theta_{ij} t_s \dot{r}(t) \tag{9}$$

where h_{3ij} is the piezoelectric voltage-strain coupling tensor, θ_{ij} is the constant solution tensor (see Alghamdi, 1995), z_m and y_m are the coordinates of the mid-point of the sensor and t_s is the sensor thickness.

The electrical voltage applied at the surface of the actuator is proportional to the derivative of the sensor potential (V_s)

$$V(x,t) = G\dot{V}_s \tag{10}$$

where G is the constant feedback gain. Substituting Equations (6) and (7) into Equation (4) and allowing arbitrary variation of $r(t)$ and $V(t)$, one obtains the following set of equations for the system,

$$M\ddot{r}(t) + C_p\dot{r}(t) + K_p r(t) + C_a V(t) = 0 \tag{11}$$

$$C_a\dot{r}(t) + S_a V(t) = q \tag{12}$$

where M, K_p, C_p, C_a, and S_a are the mass, stiffness, passive structural damping, active electro-mechanical damping, and capacitance, respectively, and q is the applied charge at the surfaces of the actuators. Details of these terms can be found in Alghamdi (1995).

The value of $V(t)$ in the actuator equation [Equation (11)] is calculated using Equations (9) and (10). The sensor equation [Equation (12)] relates the applied voltage and the mechanical displacement rate to the surface charges.

Substituting Equations (9) and (10) into Equation (11),

$$M\ddot{r}(t) + [C_p + C_a G^T]\dot{r}(t) + K_p r(t) = 0 \tag{13}$$

where G^T is the total feedback gain representing feedback gain (G) and the appropriate piezoelectric coupling coefficient.

For harmonic motion, the magnitude of the frequency response function (FRF) of the system is

$$\alpha = \frac{1}{\sqrt{(K_p - \omega^2 M)^2 + [\omega(C_p + C_a G^T)]^2}} \tag{14}$$

The phase shift of the FRF is given by

$$\theta = \tan^{-1}\frac{-\omega(C_p + C_a G^T)}{\sqrt{K_p - \omega^2 M}} \tag{15}$$

where ω is the angular excitation frequency.

Table 1. Material properties of the host.

Modulus of elasticity	2.4 (GPa)
Poisson's ratio	0.3
Density	1200 (Kg/m^3)

ANALYTICAL RESULTS

The goal of this simple dynamic analysis is to show the capability of eigenstrain techniques to model the response of active structures, in particular active damping. The active term (C_a) in Equation (13) acts as an adaptive damping term because feedback voltage $V(t)$ is made proportional to the strain rate measured by sensors. Adaptive damping is investigated for a variety of parametric changes, including variation of number of devices, device size, host stiffness, feedback gain, device position with respect to beam mid-plane and device shape. Material properties of the host and the PZT devices are given in Tables 1 and 2.

Figure 3 shows the dimensions of the adaptive beam modeled in this study. Unless otherwise stated, the following is assumed: (1) Maximum number of device-pairs (n) is four; (2) maximum device density is 2%, in order to minimize the mechanical interactions between the devices; (3) each device is placed halfway between the mid-plane and the free surface; 4) maximum feedback gain (G) is 20 and the corresponding electric field at the first pair is 526 V/mm, to avoid nonlinear response and PZT depoling; and (5) device aspect ratio ($a2/a3$) is eight. The change in the peaks of the frequency response function of the damped system in frequency domain, along with decay envelopes and damping time are presented as measures of active damping.

Effect of Number of Device-Pairs

In Figure 4, decay envelopes are plotted at constant feedback gain ($G = 19$) for different values of device-pairs ($n = 0$,

Table 2. Material properties of piezoceramic (PZT-5H).

Dielectric permittivity, ε_{33}^T	301 (10^{-10} F/m)
ε_{33}^S	130 (10^{-10} F/m)
ε_{11}^T	277 (10^{-10} F/m)
ε_{11}^S	151 (10^{-10} F/m)
Piezoelectric strain coupling, d_{31}	–274 (10^{-12} m/V)
d_{33}	593 (10^{-12} m/V)
d_{15}	741 (10^{-12} m/V)
Elastic compliance (@ constant E), S_{11}^E	16.5 (10^{-12} m^2/N)
S_{33}^E	20.7 (10^{-12} m^2/N)
S_{44}^E	43.5 (10^{-12} m^2/N)
S_{12}^E	–4.78 (10^{-12} m^2/N)
S_{13}^E	–8.45 (10^{-12} m^2/N)
Density	7500 (kg/m^3)

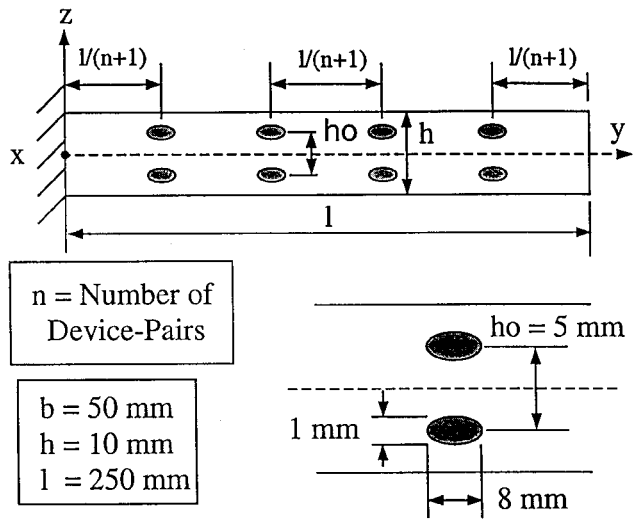

Figure 3. *Dimensions of the modeled adaptive cantilever beam.*

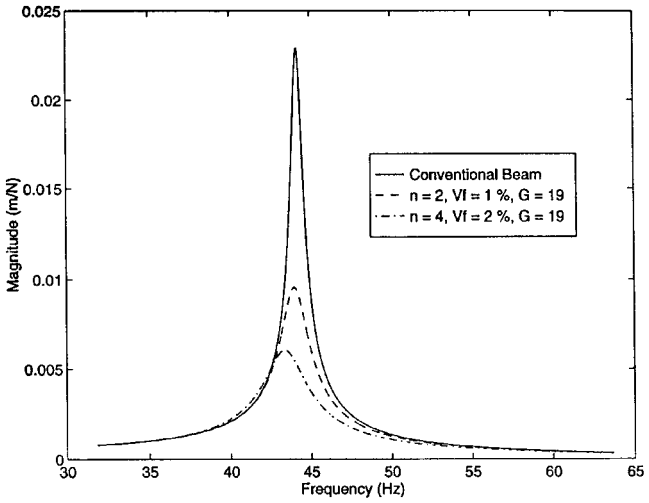

Figure 5. *Effect of increasing number of device-pairs on adaptive damping in frequency domain.*

2, 4), and the corresponding volume fractions are 0, 0.5 and 2%. For $n = 1$, the first device-pair from the fixed end is activated. The solid line represents the decay envelope of a conventional beam with no embedded devices. The adaptive beam damps faster as the number of device-pairs increases. Figure 5 shows the frequency response function (FRF) of the adaptive beam with $n = 0$, 2 and 4. The peak amplitude of the magnitude of FRF decreases as the number of active device-pairs increases. The shift in the location of the first resonance peak is attributed to the changes in the system dynamic variables (stiffness and mass). In Figure 6, adaptive damping is represented in terms of the normalized time-to-damp (t_d) vs. the number of device-pairs. Time-to-damp is defined in this paper as the time required for the tip displacement to drop to 1% of the applied initial condition. The time-to-damp of the active beam is normalized with respect to the time-to-damp of a passive beam with zero gain ($G = 0$). As expected, the rate of change in time-to-damp decreases as n increases, because the authority of additional device pairs decreases as the distance from the fixed end increases.

Effect of Device Density

Figures 7 and 8 represent adaptive damping for different device densities achieved by changing device size while the number of active device-pairs (m) is held constant ($n = 4$). In Figure 7, the time response is given as a function of the device volume fraction at constant feedback gain. Adaptive damping improves as the device volume-fraction increases, in a nonlinear way, as shown in Figure 8. The rate of change of t_d, with respect to V_f, increases up to $V_f = 0.8\%$ and then decreases with increasing V_f. This is due to both the nature of

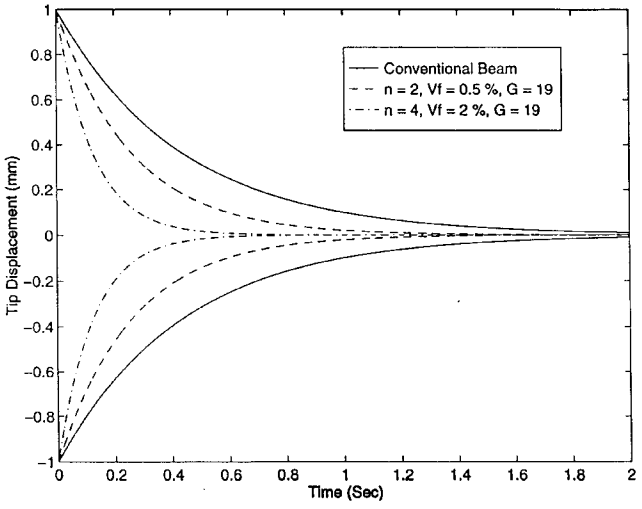

Figure 4. *Effect of increasing number of device-pairs on adaptive damping.*

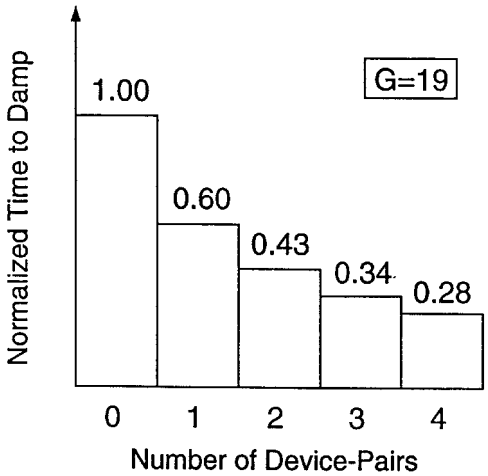

Figure 6. *Relationship between time-to-damp and number of device-pairs.*

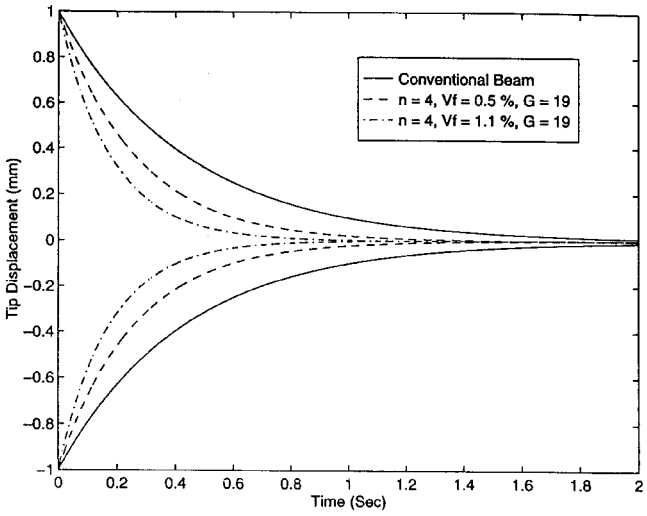

Figure 7. *Effect of increasing of device density on adaptive damping.*

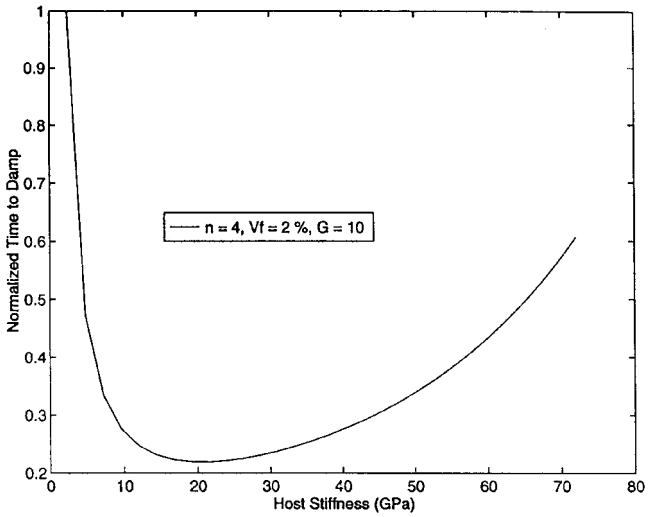

Figure 9. *Time-to-damp as a function of host stiffness.*

the damping process and the increase in device volume-fraction.

Effect of Host Stiffness

The effect of changing host stiffness on adaptive damping is shown in Figures 9 and 10. The host stiffness is changed from that of Alplex to that of aluminum while other variables are held constant. Adaptive damping increases, and then decreases, with increasing host stiffness. Similar to adaptive stiffening (Alghamdi and Dasgupta, 2000), there is an optimum host stiffness value for which adaptive damping is maximum, and it is 22 GPa for the beam considered in this paper, as shown in Figure 9. Similarly, the electrical field at the actuator of the first device-pair (E_{max}), which is proportional to the strain rate at the sensor of the first device-pair, increases from 263 V/mm at host stiffness 2.4 GPa to 1029 V/mm at 34 GPa, then decreases to 779 V/mm at host stiffness of 72 GPa, as shown in Figure 10.

Effect of Feedback Gain

Figures 11 and 12 show the effect of feedback gain (G) on adaptive damping. The decrease in the first resonance amplitude, which is a measure of adaptive damping, is shown in Figure 11 for $G = 0$, 10 and 20. The phase shift is shown in Figure 12. In both figures, there is no shift in the first natural frequency of the system as the feedback changes from 0 to

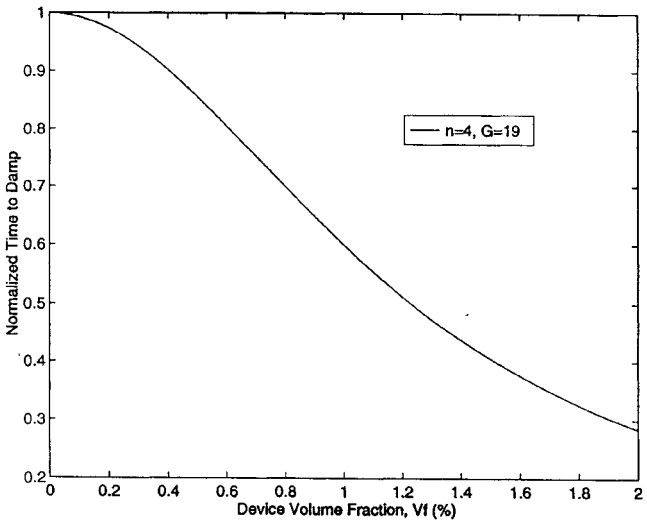

Figure 8. *Time-to-damp as a function of device density.*

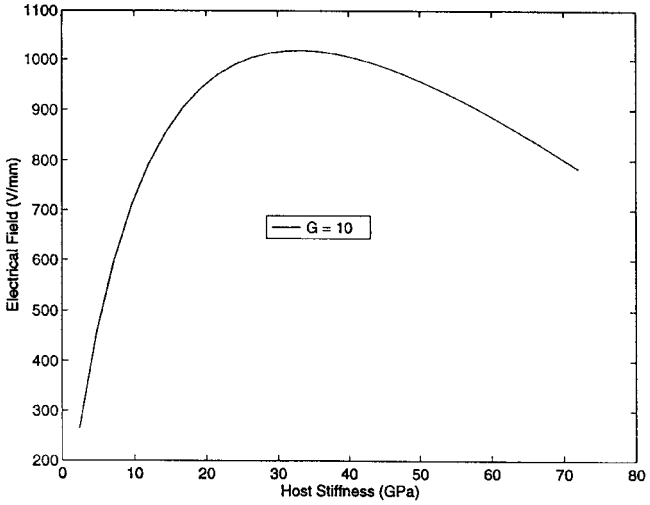

Figure 10. *Electrical field at the actuator of the first device-pair (E_{max}) as a function of host stiffness.*

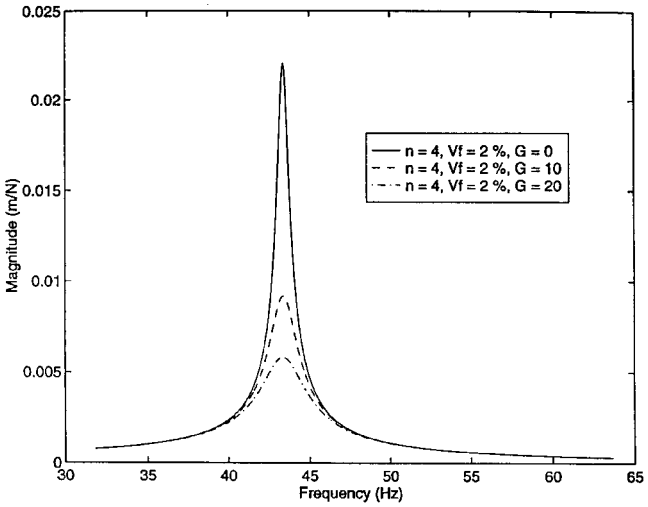

Figure 11. *Effect of feedback gain on adaptive damping in frequency domain (magnitude).*

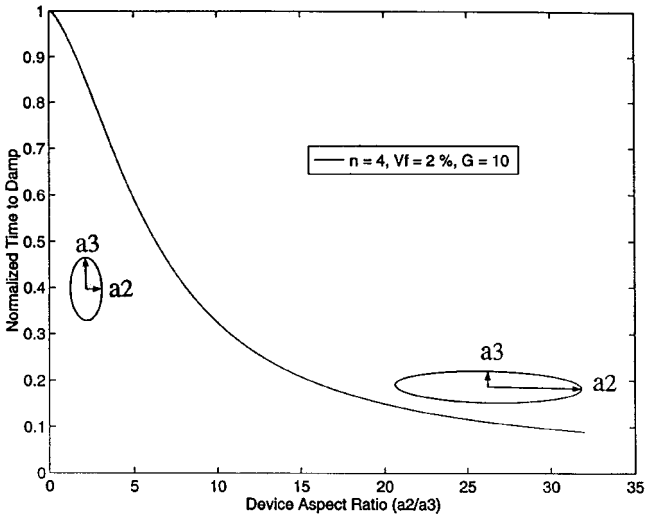

Figure 13. *Time-to-damp as a function of device shape.*

20, because there is no change in either mass or stiffness of the system.

Effect of Device Shape

Figure 13 illustrates the effect of changing the device shape on adaptive damping. Changing the aspect ratio $a2/a3$ changes device shape, where $a2$ and $a3$ are the device semi axes. It is seen in this figure that increasing the aspect ratio helps to damp the system faster, because actuators, as well as sensors have more authority at higher aspect ratios. However, as the aspect ratio increases, the time-to-damp decreases and reaches some saturation value. The role of the aspect ratio is fairly limited beyond this value.

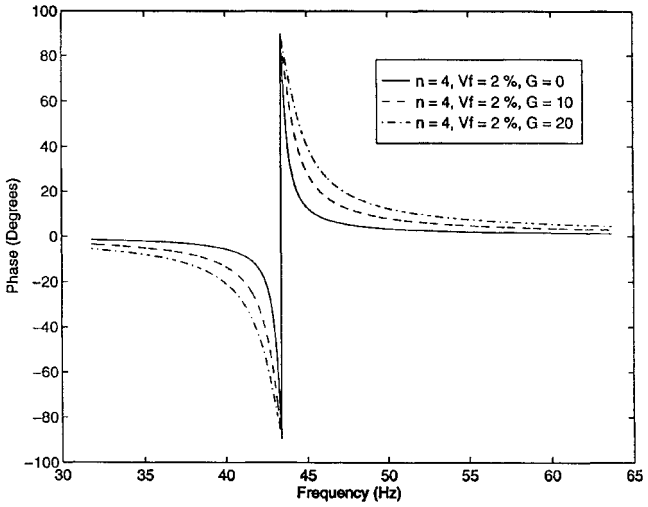

Figure 12. *Effect of feedback gain on adaptive damping, in frequency domain (phase).*

Effect of Device Location

Finally, the effect of device location on adaptive damping is investigated in Figure 14 by changing the distance of the device centerline from the beam mid-plane. Time-to-damp is normalized with respect to that of a passive beam with devices not activated. As expected, moving devices away from beam mid-plane improves systems adaptive damping because of the increase in the device authority. Normalized device location from beam mid-plane is donated by l_o. For $l_o = 0.3$, sensor and actuator are closer to the beam mid-plane and their ability to damp the beam is minimal. As the centerline of the device moves to half the distance between mid-plane and the free surface ($l_o = 0.5$), the capability of the actuators to damp the beam improves. However, as the embedded de-

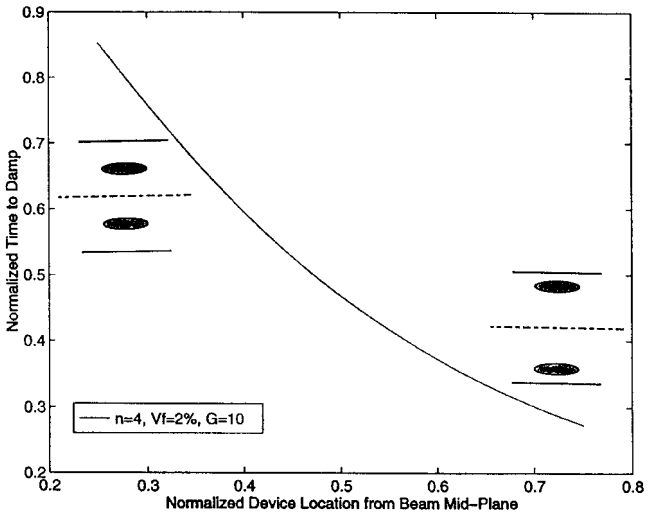

Figure 14. *Time-to-damp as a function of device location.*

vices reach the free surfaces, the free effect of the boundary has to be addressed. In other words, the assumption of mini-devices in an infinite matrix breaks down. In such a situation the Green's functions in the eigenstrain method need to be modified.

EXPERIMENTAL VERIFICATION

Experimental verification of the eigenstrain models developed above is presented in this section. An adaptive cantilever beam was fabricated. Figure 15 shows the dimension of the beam, as well as the dimensions of the embedded devices. Device location (l_o) is 0.29. Material properties of the host and the PZT devices are given in Tables 1 and 2. Method of fabrication of this adaptive beam can be found in Alghamdi (1995). The beam has four built-in device-pairs ($n = 4$). Each pair consists of a sensor and actuator. So, in principle it is possible to activate all of these pairs, i.e. $m = 4$.

As mentioned before, the reason for choosing small devices is to reduce the obtrusivity and hence promote better structural integrity of the device. Thus, the experimental study of the active structure presented in this paper is different from most of the published articles, see for example (Crawley and de Luis, 1987; Baz and Ro, 1995). This is because sensors and actuators are relatively small, in comparison to devices used by other researchers. Dimensions of the piezoelectric elements are at least one order of magnitude less than the dimensions of the cantilever beam in the y-z plane, as shown in Figure 15.

Only the first two pairs of devices in Figure 15 from the fixed end are used for active vibration control, while the third pair is used to excite the beam during forced vibration tests. Devices of the fourth pair are not used in this setup, because the amount of strain (or voltage output) measured at the fourth pair is too small for the cantilever beam configuration. Nevertheless, this pair could be useful if the active beam is used in other configurations like simply-supported or fixed-fixed boundary conditions. An external piezoceramic element having the same dimensions as the embedded devices is bonded to the external surface of the beam 8 mm from the fixed end of the beam, as shown in Figure 15. This PZT is used as a general sensor because interactions between stress fields of sensor and actuator were encountered in experimental work while ignored in the developed model.

The feedback system is shown in Figure 16 for the frequency response test. It consists of a voltage pre-amplifier connected to the external PZT sensor. The pre-amplifier is connected to a 3202 Krohn-Hite low-pass frequency filter, to filter out noises generated in the system. The signal coming out of the frequency filter is sent to two different circuits leading to the actuators of the first and the second device-pairs. Each loop is designed to condition the signal before it goes to the actuator of the proper device-pair. The frequency filter is connected to two different phase shifters. The phase shifter is used to adjust the phase between sensor output voltage and the voltage sent to the actuator. The phase shifter is adjusted manually at an excitation frequency equal to the first natural frequency of the beam.

A differentiator is connected to the phase shifter to make the applied electrical field in the actuator proportional to the sensor output voltage rate. A Crown Comp-Tech 400 power amplifier is connected to the differentiator to amplify the signal before it goes to each actuator.

The experimental value of the feedback gain in each sensor-actuator circuit is computed as the ratio between the actuator voltage V_a and the sensor voltage V_s (Alghamdi and Dasgupta, 2000). In forced vibration tests, a sweep sinusoidal voltage of amplitude of 5 V is generated using a Spectrum Analyzer (HP 35665A). This signal is amplified to 120 V using a power amplifier (Crown Comp-Tech 400), and applied to the third pair. The two devices of the third pair are driven 180° out-of-phase in order to drive the beam in pure bending.

The frequency response is measured using the Spectrum Analyzer which compares the voltage input to the devices of the third pair, with the output voltage measured at the exter-

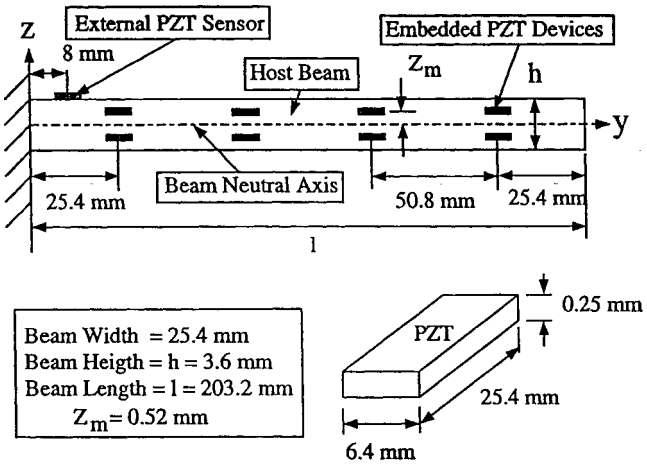

Figure 15. *Dimensions of the fabricated adaptive beam.*

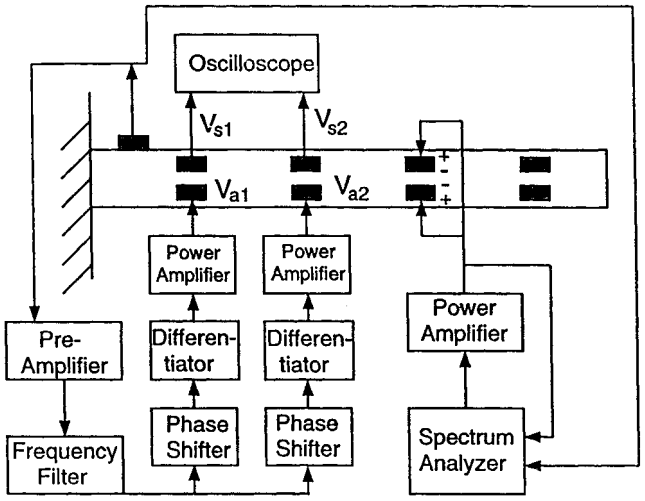

Figure 16. *Experimental setup for forced vibration tests.*

nal attached PZT sensor, as shown in Figure 16. Experimental frequency response data is recorded by the digital Spectrum Analyzer and then downloaded to a computer for analysis and post-processing. Time response is measured by connecting the external PZT to an oscilloscope while no voltage is applied to the devices of the third pair. The tip of the beam is given some fixed initial displacement (r_o) and the beam is allowed to vibrate under active vibration control. The time response of the active beam is captured by an oscilloscope (Nicolet 320 Digital Oscilloscope).

In active damping, the electrical field applied to the actuator is proportional to the rate of the sensor voltage. The electrical field supplied to each actuator is 180° phase shifted with respect to the electrical field generated by the sensor of that pair. In principle, it is possible to use sensors of the first two pairs as additional actuators. However, because of mechanical interaction effects, only one device of each pair is used as an actuator. Since the model does not account for the mechanical interactions between opposite devices in each pair, using them simultaneously as actuators would make it difficult to compare experimental results with analytical predictions.

Figure 17 illustrates experimental measurements of the free vibration of the adaptive beam in time domain. The figure shows the effect of increasing feedback gain on the experimental time response at constant active pairs ($m = 2$). As expected, the beam damps faster as the feedback gain increases from 0 to 58 (at $G = 58$ the corresponding electrical field is 180 V/mm which is way below the depoling value). The frequency of vibration remains relatively unaltered in comparison to adaptive stiffening (Alghamdi and Dasgupta, 2000). The experimental frequency response (forced vibration) of the adaptive beam is shown in Figure 18. In this figure, the x-axis is the sweep excitation frequency in Hz and the vertical axis is the ratio between the output voltage of the external PZT sensor and the excitation voltage at the devices of the third pair. Unlike the time domain response, number of active pairs (m) is being changed at constant gain ($G = 174$, $E = 530$ V/mm). The location of the first resonance remains relatively constant at 24.50 Hz. Adaptive damping is illustrated by the decrease in the peak amplitude of the FRF. The contribution of the second pair is less than that of the first pair because the latter one has more authority for the cantilever beam configuration. The heat generated in the PZT actuators is minimal because the excitation frequency is always less than 30 Hz, both in the forced and free vibration tests. In other words, since the aim is to control the response of an adaptive beam having first natural frequency approximately 25 Hz, the heat generated at this frequency will be dissipated to the structure at an acceptable rate. There was no visual or apparent change in the temperature of the adaptive beam due to the excitation of the PZT actuator. However, for higher excitation frequency, above 100 Hz, one should account for the heat generated in PZT to avoid matrix softening and/or degradation of piezoelectricity effect.

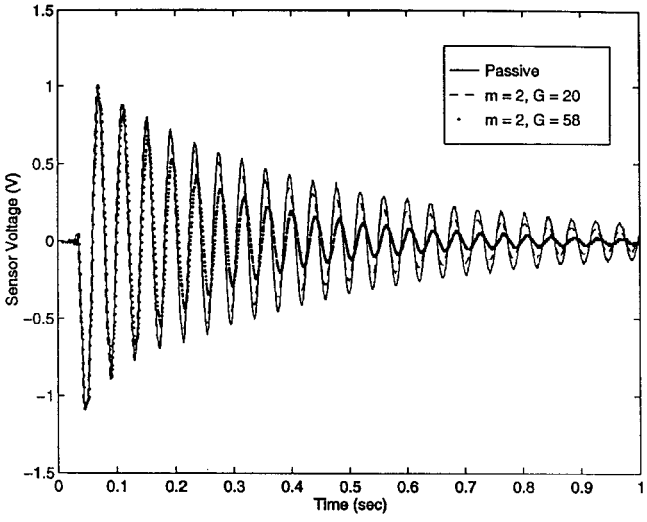

Figure 17. *Effect of increasing feedback gain on experimental adaptive damping in time domain.*

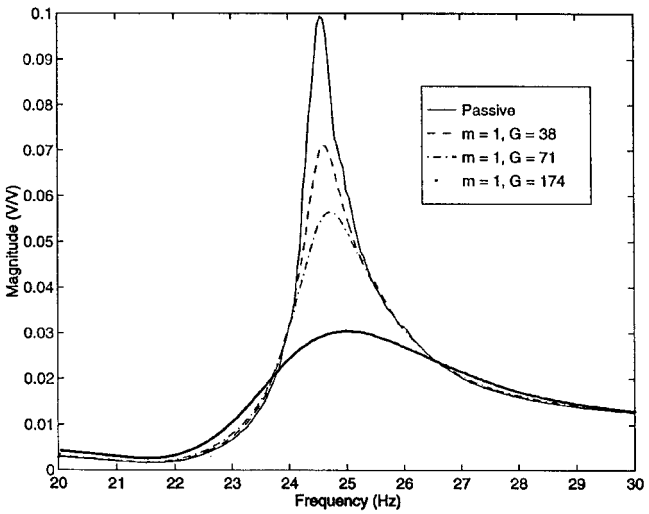

Figure 18. *Effect of increasing feedback gain on experimental adaptive damping in frequency domain.*

Some deviation between experimental results and analytical predictions is acceptable, due to the simplifying assumption made in the model, such as: perfect interfacial bonding condition is assumed in the model, the rectangular cross section of the devices is approximated to be elliptical with equivalent areas in the analytical model, the electrical losses in the system are ignored in the model, the finite dimensions of the host in the z direction are considered very approximately in the eigenstrain analysis, mechanical interactions between the embedded devices are ignored in the model, the sensor outputs are estimated in the experiment from the external PZT sensor, and the nonlinearities in the material properties of the devices have been ignored. Because of the difficulties in accounting for these approximations explicitly, a scalar calibration coefficient (k) is assumed in the

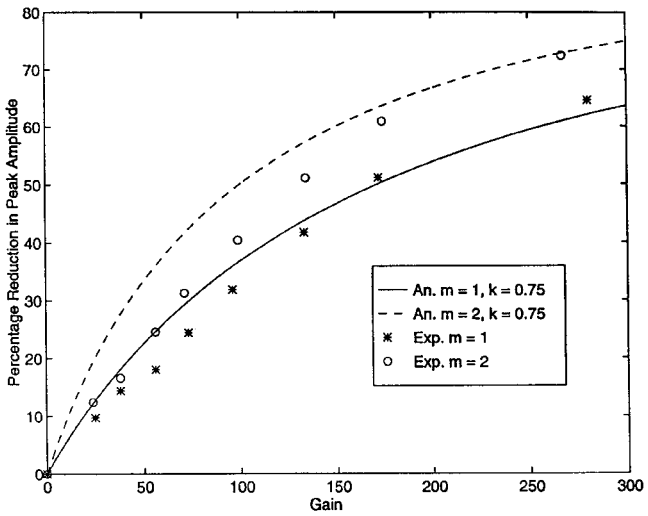

Figure 19. *Comparison between analytical and experimental adaptive damping, represented by the percentage reduction resonance peak amplitude, assuming losses in the system.*

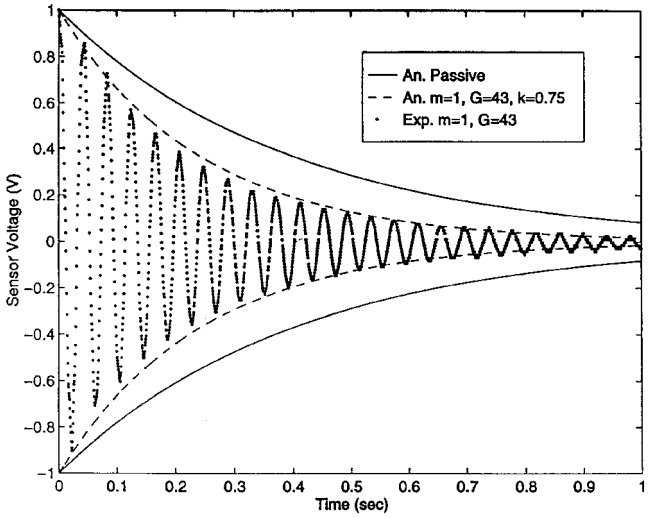

Figure 21. *Comparison between analytical and experimental adaptive damping for* m *= 1, in time domain.*

model to simulate the effects of the above simplifications in the model. One can estimate the value of the coefficient based on some simple experimentation. The beam is given a known tip displacement and the voltage output of an embedded sensor is recorded. Sensor voltage output is compared with the analytical prediction. The experimental value is 75% of the analytical prediction. This implies that the overall electro-mechanical efficiency of the embedded devices is 75% in the static case.

Figure 19 gives a comparison between the analytical and experimental frequency response results for $m = 1$ and $m = 2$. The adaptive damping is measured as the percentage reduction in the peak amplitude of the first resonance, and it is plotted against the feedback gain (G). The experimental values of the feedback gain are the ratios between the applied voltage at the actuator and the corresponding sensor voltage, as estimated by equation 16 in Alghamdi and Dasgupta (2000). In this plot, the analytical results are scaled down by the empirical correction factor $k = 0.75$.

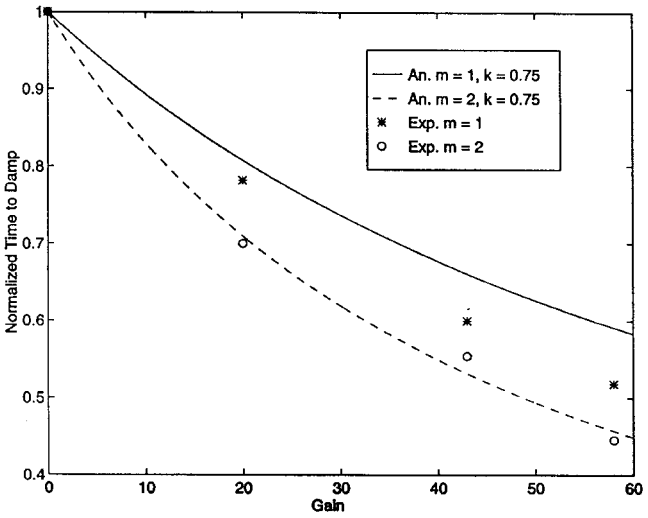

Figure 20. *Comparison between analytical and experimental time-to-damp, assuming losses in the system.*

Figure 20 shows a comparison between the experimental time-to-damp and the analytical prediction for $m = 1$ and 2, at different gains (assuming a correction factor $k = 0.75$). Reasonable agreement is obtained in the relative trends. The comparison between the experimental results and model predictions in time domain is given in Figure 21. The y-axis is the normalized external sensor output measured experimentally or predicted analytically. Analytical and experimental time responses are given for $m = 1$ and $G = 43$ ($E = 130$ V/mm). The solid line represents the analytical passive decay envelope, whereas the dashed line is the analytical decay envelope for $m = 1$, $G = 43$ and $k = 0.75$. The dotted line is the normalized sensor voltage representing the displacement of the beam. Again, the ability to achieve good agreement between experimentally measured and analytically predicted response with use of only one fixed scalar calibration factor ($k = 0.75$) illustrates the ability of the eigenstrain method to represent the basic mechanics of the active structure with embedded mini-devices.

It is worth mentioning in closing that significant tuning in the damping behavior of the adaptive beam was achieved using a small volume fraction of the devices (which is only 0.22% for each actuator).

CONCLUSIONS

This paper, along with a previous one (Alghamdi and Dasgupta, 2000) in this two-part series, has demonstrated for the first time a unified approach, based on eigenstrain techniques, for modeling the mechanics of distributions of

mini-devices embedded in an electromechanical smart structure. Sensors are treated as elastic heterogeneities subjected to external loads, while actuators are treated as elastic heterogeneities subjected to both external loads and internal induced strain caused by the converse piezoelectric effect. The Hamilton energy functional of the adaptive structure is evaluated using an appropriate variational scheme. Numerical results, using the Raleigh-Ritz scheme, show the capability of eigenstrain techniques to capture the physics of adaptive damping under a variety of parametric changes such as gain factor and device densities. The trends predicted by the proposed models provide reasonable qualitative agreement with the experimental results. By assuming a scalar empirical calibration factor, fair agreement is obtained between analytical prediction and experimental results.

ACKNOWLEDGEMENTS

This work has been partially supported by the Army Research Office under their University Research Initiative. The program monitor is Gary Anderson.

REFERENCES

Alghamdi, A. A. A. 1995. "Response of Adaptive Structures with Multiple Embedded Devices Using Eigenstrain Techniques," Ph. D. Thesis, University of Maryland, College Park.

Alghamdi, A. A. A. and Dasgupta, A. 1993a. "Interaction Mechanics between Embedded Micro-Actuators and the Surrounding Host in Adaptive Structures," *Proceedings of North American Conference on Smart Structures and Materials,* Albuquerque, New Mexico, pp. 317–328.

Alghamdi, A. A. A. and Dasgupta, A. 1993b. "Frequency Prediction of a "Smart" Beam Using Eshelby Techniques with Linear Distributed Strains," *Proceedings of American Society for Composites, Eighth Technical Conference,* Cleveland, Ohio, pp. 174–183.

Alghamdi, A. A. A. and Dasgupta, A. 2000. "Eigenstrain Techniques for Modeling Adaptive Structures: I) Active Stiffening Tailoring, *Journal of Intelligent Material Systems and Structures,* Submitted.

Allik, H. and Hughes, T. J. R. 1970. "Finite Element Method for Piezoelectric Vibration," *International Journal for Numerical Methods in Engineering,* 2:151–157.

Bailey, T. and Hubbard, J. E. Jr. 1985. "Distributed Piezoelectric-Polymer Active Vibration Control of a Cantilever Beam," *AIAA Journal of Guidance, Control and Dynamics,* 8(5):605–611.

Baz, A. and Ro, J. 1995. "Optimum Design and Control of Active Constrained Layer Damping," *Journal of Vibration and Acoustics,* 117:135–144.

Chandrashekhara, K. and Bhatia, K. 1993. "Active Buckling Control of Smart Composite Plates: Finite Element Analysis," *Smart Materials and Structures,* 2(1):31–39.

Chee, C. Y. K. et al. 1998. "A Review on the Modeling of Piezoelectric Sensors and Actuators Incorporated in Intelligent Structures," *Journal of Intelligent Material Systems and Structures,* 9(9):3–19.

Chen, P. C. and Chopra, I. 1996. "Induced Strain Actuation of Composite Beams and Rotor Blades with Embedded Piezoceramic Elements," *Smart Materials and Structures,* 5(1):35–48.

Crawley, E. F. 1994. "Intelligent Structures for Aerospace: A Technology Overview and Assessment," *AIAA Journal,* 32(8):1689–1699.

Crawley, E. F. and de Luis, J. 1987. "Use of Piezoelectric Actuators as Elements of Intelligent Structures," *AIAA Journal,* 25(10):1373–1385.

Crawley, E. F. and Lazarus, K. B. 1991. "Induced Strain Actuation of Isotropic and Anisotropic Plates," *AIAA Journal,* 29(6):944–951.

Dasgupta, A. and Alghamdi, A. A. A. 1993. "Eshelby's Techniques for Modeling Interaction Mechanics in Adaptive Structures," *Proceedings of the Society of Engineering Science, 30th Annual Technical Meeting,* AMD Vol. 159, Charlottesville, Virginia, pp. 293–302.

Eshelby, J. D. 1957. "The Determination of the Elastic Field of an Ellipsoidal Inclusion and Related Problems," *Proceedings of the Royal Society,* Series A, 241:376–396.

Gartner, J. R. and Olgac, N. 1982. "Improved Numerical Computationing Uniform Beam Characteristic Values and Characteristic Functions," *Journal of Sound and Vibration,* 84(4):481–489.

Hagood, N. W. et al. 1990. "Modeling of Piezoelectric Actuator Dynamics for Active Structural Control," *Journal of Intelligent Material Systems and Structures,* 1(3):327–354.

Ikeda, T. 1990. "Fundamentals of Piezoelectricity," Oxford Science Publications, Oxford.

Im, S. and Atluri, S. N. 1989. "Effects of a Piezo-Actuator on a Finitely Deformed Beam Subjected to General Loading," *AIAA Journal,* 27(12):1801–1807.

Kupchinov, B. I., Ermakov, S. F., Rodnenkov, V. G., Bobrysheva, S. N., Beloenko E. D. and Kestelman, V. N. 1993. "Role of Liquid Crystals in the Lubrication of Living Joints," *Smart Materials and Structures,* 2(1):7–12.

Lin, M. W. and Rogers, C. A. 1992. "Analysis of a Beam Structure with Induced Strain Actuators Based on an Approximated Linear Shear Stress Field," *Proceedings of the Recent Advances in Active and Sensory Materials and Their Applications,* Blacksburg, Virginia, pp. 363–376.

Mahut, T. et al. 1998. "Dynamic Analysis of Piezoelectric Fiber Composite in an Active Beam Using Homogenization and Finite Element Methods," *Journal of Intelligent Material Systems and Structures,* 9(12):1009–1017.

Pratt, J. R. et al. 1999. "Terfenol-D Nonlinear Vibration Absorber," *Journal of Intelligent Material Systems and Structures,* 10(1):38-58.

Soh, C. K., Tseng, K. K.-H., Bhalla, S. and Gupta, A. 2000. "Performance of Smart Piezoceramic Patches in Health Monitoring of a RC Bridge," *Smart Materials and Structures,* 9(4):533–542.

Tiersten, H. F. 1969. *Linear Piezoelectric Plate Vibrations,* Plenum Press, New York.

Wang, B-T and Rogers, C. A. 1991. "Modeling of Finite-Length Spatially-Distributed Induced Strain Actuators for Laminated Beams and Plates," *Journal of Intelligent Material Systems and Structures,* 2(1):38–58.

Yoshida, K. Nenchev, D. N. and Uchiyama, M. 1999. "Vibration Suppression and Zero Reaction Maneuvers of Flexible Space Structure Mounted Manipulators," *Smart Materials and Structures,* 8(6):847–856.